Regional supply chains for decarbonising steel: resource efficiency and green premium mitigation

Alexandra Devlin, Aidong Yang

Department of Engineering Science, University of Oxford, Parks Road, Oxford, OX1 3PJ, United Kingdom

Supplementary Information

Table of Contents

List of Tables and Figures

A. Additional Modelling Details

A.1 Energy Pathways

Table A.1 below explicates the energy pathway, from VRE to end-use, when performed in Australia (differentiated by VRE_{on} or VRE_{off}) or Japan. Flexible processes were only supplied by direct VRE during VRE_{on} in Australia, whilst inflexible processes had an additional supply route during VRE_{off}. The energy pathway is shown for both Australia- and Japan-based production, where applicable.

Table A. 1 – Energy pathways, dependent on process flexibility and country

Process	Energy type	Flexibility	Country	Supply route - Aus (VRE_{on})	Supply route - Aus (VRE off) or Japan
Water electrolysis	Electricity (DC)	Flexible	Aus	Direct VRE	-
H_2 liquefaction	Electricity (AC)	Flexible	Aus	Direct VRE	-
CGH_2 storage compression	Electricity (AC)	Flexible	Aus	Direct VRE	-
NH_3 synthesis	Electricity (AC)	Inflexible	Aus	Direct VRE	CGH_2-FC
NH_3 cracking	Thermal	Inflexible	Jpn	-	VRE-Electrolysis-NH_3
DRI	H_2 feedstock	Inflexible	Aus	Direct VRE	VRE-Electrolysis-CGH_2-FC
	H_2 feedstock	Inflexible	Jpn	-	VRE-Electrolysis-LH_2/NH_3-regasification/cracking
H_2 compression pre-DRI	Electricity (AC)	Flexible	Aus	Direct VRE	-
	Electricity (AC)	Inflexible	Jpn	-	VRE-Electrolysis-LH_2/NH_3-FC
H_2 heating pre-DRI	Electricity (AC)	Inflexible	Aus	Direct VRE	-
	Thermal	Inflexible	Aus	-	VRE-Electrolysis-CGH_2-combustion
	Thermal	Inflexible	Jpn	-	VRE-Electrolysis-LH_2/NH_3-combustion
EAF	Electricity (AC)	Inflexible	Aus	Direct VRE	VRE-Electrolysis-CGH_2-FC
	Electricity (AC)	Inflexible	Jpn	-	VRE-Electrolysis-LH_2/NH_3-FC
Casting	Electricity (AC)	Inflexible	Aus	Direct VRE	VRE-Electrolysis-CGH_2-FC
	Electricity (AC)	Inflexible	Jpn	-	VRE-Electrolysis-LH_2/NH_3-FC
Marine transportation	Electricity (AC)	Inflexible	Aus	Direct VRE	VRE-Electrolysis-CGH_2-FC
	Electricity (AC)	Inflexible	Jpn	-	VRE-Electrolysis-LH_2/NH_3-FC

A.2 Homer Pro energy calculations

Total daily electricity demand was inputted as deferrable load in Homer Pro, the sum of all system demands (excluding external iron ore mining and water desalination processes). All loads were converted to DC due to the pairing of solar electricity DC outputs and the central electrolyser DC load. System flexibility of 5% unmet electric load was given to rationalise for the constant daily load profile throughout the year, hence the lack of seasonal production consideration. If we had adopted a seasonally variant diurnal demand profile by minor adjustment of the assumed steel output, this 5% unmet electric demand would likely not be needed to achieve similar LCOE to what is currently projected.

The deferrable peak load, required by Homer Pro, was determined by:

$$Peak\ load\ (kW) = daily\ load\ (kWh/d)/VRE_{on}\ (hrs/day) \quad (A.1)$$

The storage capacity (a system flexibility constraint, required by Homer Pro) differed according to the case. For SC1-LH_2, as all loads were flexible, no restrictions existed for when load could be served, therefore

$$Storage\ capacity_{SC1\text{-}LH2}\ (kWh) = daily\ load\ (kWh) \quad (A.2)$$

Otherwise, inflexible processes restricted supply and the storage capacity was determined by the flexible CGH_2 and LH_2 storage:

$$Storage\ capacity_{SC2\text{-}LH2,\ SC3\text{-}LH2}\ (kWh) = energy\ needed\ to \quad (A.3)$$
$$(a)\ produce\ the\ H_2\ to\ be\ stored\ by\ CGH_2\ and\ LH_2,\ and$$

(b) run the compression for operating CGH_2 and liquefier for operating LH_2

Storage capacity$_{NH3}$ (kWh) = energy needed to (A.4)
(a) produce the H_2 to be stored by CGH_2 and
(b) run the compression for operating CGH_2

A.3 Aspen Plus calculations

A.3.1 The DRI process

The DRI process outlined in Figure A.1, following the design of Krüger et al. (2020), was simulated in Aspen Plus using the SOLIDS property method. The reduction furnace was modelled by a adiabatic RStoic reactor (primarily for heat balance calculations), using surplus H_2 as heat carrier (with heat supplied through the pre-DRI H_2 heater, following an exchanger for heat recovery) to sustain the reduction reactions. Pressure drop in the furnace was considered, through a pre-DRI compression step to raise the pressure from 1 bar to 2 bar, although the operating pressure of the furnace was taken as 1 bar as a simplifying approximation. To estimate the temperature of the gaseous product of the furnace for an intended solid product temperature (850 °C) that is expected to materialise in a adequately designed furnace, a heater (cooler) was applied to the solid (gaseous) product (not shown in Figure A.1). The heater was specified with the intended solid product temperature (see Table A.2) while the cooler's duty was set to be identical to that of the heater (through imposing a design specification in Aspen Plus). This way, the heat balance of the furnace was maintained.

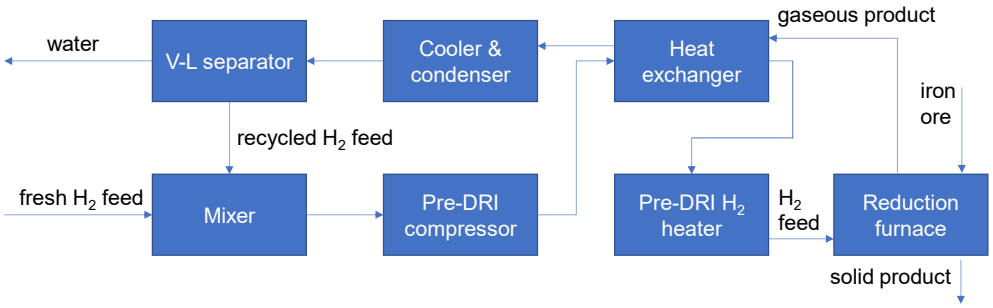

Figure A. 1 – Block diagram of the DRI process simulated in Aspen Plus

Key simulation settings and results are given in Table A.2. Note that the above-described process has a high-temperature output of reduced iron, ideal for directly feeding into the down-stream EAF process. In supply chain SC2, the thermal energy contained in the hot DRI product flow would not enter the EAF as the two processes were at different locations; the implications of this difference, as well as the requirements of the briquetting process, were ignored in this study. Furthermore, mass losses of iron were not considered in the conversion from sponge iron (Fe/FeO) to liquid steel (LS), then semi-finished steel (SFS).

Table A. 2 – Aspen Plus simulation details for the DRI process

Simulation settings	
Iron ore feed rate and temperature	1500 kg/hr, 20 °C
Composition of iron ore (weight%)	95% of Fe2O3, 5% of inert (represented by SiO2)
Furnace operating pressure	1 bar
Metallisation (FeO to Fe conversion) rate	94%
Fresh H_2 feed rate, temperature and pressure	51.4 kg/hr, 80 °C, 1 bar
H_2 conversion rate in furnace	30.5%
Solid product temperature	850 °C

“H_2+steam” stream condensing temperature	40 °C
Results	
H_2 heating requirement	0.4446 MW
H_2 compression work requirement	0.0642 MW
Temperature of gaseous outlet flow of the furnace	338 °C
Solid products	Fe = 936.9 kg/hr; FeO = 76.9 kg/hr; SiO2 =75 kg/hr

A.3.2 NH_3 cracking

The NH_3 cracking reactor was modelled in Aspen Plus with the RStoic reactor model and the SKR physical property model. The reactor was assumed to operate isothermally. Before entering the reactor, liquid NH_3 was assumed to be pumped and pre-heated to the reactor conditions (see Table A.3). Following pumping and prior to preheating, the NH_3 feed was assumed to reach 20 °C in gaseous state by absorbing heat from the ambient environment, free of energy cost. Heat recovery from cooling the reactor effluent and from the combustion of unconverted NH_3 and unrecovered H2 was considered to counterbalance the heat required for pre-heating the feed and for maintaining the temperature of the endothermic cracking reaction. The pumping energy requirement was negligible compared to the heating demand and was therefore not included in the assessment.

Key simulation and calculation settings (similar to those adopted in (Giddey et al., 2017) results are given in Table A.3.

Table A. 3 – Simulation and calculation details for NH_3 cracking

Simulation/calculation settings	
Reactor temperature	400 °C
Reactor pressure	8 bar
NH_3 cracking conversion	95%
H_2 product recovery	85%
Heating efficiency	85%
Target temperature of reactor effluent cooling for heat recovery	80 °C
Effective heat recovery ratio (from combustion of residual NH_3 and H_2 and from reactor effluent)	85%
Results – per tonne NH_3 feed	
Total heating requirement	4556.47 MJ
Sensible heat recovered from reactor effluent	925.97 MJ
Heat recovered from the combustion of residual NH_3 and H_2	3370.44 MJ
Net heating requirement	260.05 MJ (0.072 MWh)

A.3.3 CGH_2 compression work

Compression of H_2 was modelled via a 5-stage compressor with equal pressure ratio, inter-stage cooling temperature = 50 °C, isentropic efficiency = 85%, mechanical efficiency = 95%, physical property model = SRK.

A.4 Shipping fuel consumption calculations

Specific fuel consumption (SFC) was particular to the vessel propulsion system, calculated according to Equation (A.5). We have taken an average 85% propulsion load factor; a measure of the load the fuel cell is operating at, in relation to the specified maximum continuous rating (SMCR). Note that PEMFC runs most efficiently at 10-25% load factor whilst SOFC runs most efficiently at 25-35% load factor.

$$SFC\ (g/kWh) = \frac{correction\ factor}{LHV_{fuel}\left(\frac{kW}{kg}\right) \div 1000\ \frac{g}{kg} \times \eta} \qquad (A.5)$$

where:

correction factor = 1.19 for PEMFC and 1.09 for SOFC (Kim et al., 2020) based on 85% propulsion load
LHV = 33.33kWh/kg for H_2, 5.17kWh/kg for NH_3
η = propulsion system efficiency (fuel cell (68% in 2030, 72% in 2050), inverter (95%), and electric motor (98%))

The fuel consumption due to propulsion load was specific to the vessel propulsion system and route, calculated by:

$$F_{journey}\ (t/journey) = [SFC\ \left(\frac{g}{kWh}\right) \times\ power\ (kW) \times \frac{distance\ (nm/journey)}{speed\ \left(\frac{nm}{h}\right)} \times\ 10^{-6}\left(\frac{t}{g}\right) \div (1 -\ BOG\ (\%))]\ x\ 2 \qquad (A.6)$$

where:
power = propulsion power at 85% SMCR, i.e., 15% specified engine margin
distance = nautical distance from Port Hedland to Osaka + 15% sea margin
speed = speed of vessel
BOG = portion of initial mass lost over journey due to boil off gas, calculated using 0.2%/day for LH_2 (Wijayanta et al., 2019) and 0.02%/day for NH_3 (Al-Breiki & Bicer, 2020b). BOG losses were conservative for fuel as the decreasing daily mass due to consumption of fuel is not considered.

Shipping vessel specifications are detailed in Table A.4. Note that propulsion power was later equalised on an 85% SMCR basis by Equation (A.7):

$$Power_{85\%SMCR} = Power_{X\%SMCR} \times \frac{85}{X} \qquad (A.7)$$

Table A. 4 – Shipping vessel specifications

Export	Vessel	dwt	Power (kW)	Specified engine margin	Speed (nm/h)	Reference
Iron ore	Dry bulk carrier Newcastlemax	205000	17180	10%	14.7	(MAN Diesel and Turbo, 2014)
HBI, steel	Dry bulk carrier, Panamax	75000	9470	10%	14.5	(MAN Diesel and Turbo, 2014)
LH_2, LNH_3	Liquefied gas tanker, 160,000m3	31000	27000	0%	18	(Yoshino et al., 2012) (Al-Breiki & Bicer, 2020b)

The propulsion load factor is distinct from the cargo carrying capacity. The former refers to the engine output whilst the latter refers to the amount of usable vessel space for exported goods. We have assumed a cargo carrying capacity of 90%. Both the laden (with cargo) and ballast (without cargo) journeys are considered. In the ballast journey, water effectively replaces the weight of cargo and equal propulsion power is required. The number of journeys is specific to the vessel, export and year, calculated by:

$$journeys_{dry\ bulk}\ (no./year) = (total\ annual\ exports)\ (t) \div payload_{dry\ bulk}\ (t/vessel) \qquad (A.8)$$

$$journeys_{gas\ tanker}\ (no./year) = (total\ annual\ exports + BOG\ losses)\ (t) \div payload_{gas\ tanker}\ (t/vessel) \qquad (A.9)$$

where:
$payload_{gas\ tanker}$ (t) = 160,000m3 x ρ_{fuel} (kg/m^3) x 90%
$payload_{dry\ bulk}$ (t) = ((dwt x 90%) – $F_{journey}$) x 90%

The journey duration is a function of the vessel speed:

$$duration\ (days) = distance\ (nm/journey) \div speed_{vessel}\ (nm/h) \div 24\ (h/day) \quad (A.10)$$

The number of journeys and each journey's duration can then be used to determine the number of vessels in a fleet:

$$vessels\ in\ fleet\ (no.) = (journeys\ (no.) \times (duration\ (days) + 2) \times 2) \div 365.25 \quad (A.11)$$

A.5 Combined energy data and formulae

Table A.5 specifies the energy demand formulae for end-uses powered by direct VRE or an energy vector (H_2 or NH_3); the latter has been separated into key categories: H_2 for feedstock, H_2 or NH_3 for power, H_2 or NH_3 for heat, and H_2 or NH_3 for mobility.

Energy consumption from H_2/NH_3 demand was determined using Equation (A.12) or (A.13):

$$E\ (MWh) = H_2\ demand\ (t) \times electrolysis\ energy\ demand\ (MWh/t\ H_2) \quad (A.12)$$

$$E\ (MWh) = H_2\ demand\ (t) \times H_2/NH_3\ (t/t) \times electrolysis\ energy\ demand\ (MWh/t\ H_2) \quad (A.13)$$

where:
H_2/NH_3 = mass conversion rate
= 0.002(g H_2/mol) ×1/0.017 (g NH_3/mol) × 3/2 (moles H_2/moles NH_3)
= 0.176 (i.e., H2 constitutes 17.6% of ammonia by mass)

Note that VRE_{on} and VRE_{off} are only specified for inflexible processes in Australia which require constant load, 2030 and 2050 are only specified for processes which change in energy demand over time, and steel refers to semi-finished product (bloom, billet, or slab).

Table A. 5 – Energy modelling formulae

Direct VRE (AU): *E_{annual} (MWh) = demand rate (MWh/t) x quantity (t H_2/NH_3/SFS)*						
Applicable processes	Energy vector	SC	Unit	Demand (MWh/unit)	Source	Qty (annual basis)
H_2 liquefaction	LH_2	SC1,2,3	t H_2	10 (2030) 6 (2050)	Berstad et al. (2019)	H_2 for export and shipping fuel
NH_3 synthesis (VRE_{on})	NH_3	SC1,2,3	t NH_3	0.7	Nayak-Luke et al. (2018)	NH_3 for export and shipping fuel x (VRE_{on} (hrs)/24)
CGH_2 storage compression	LH_2	SC2	t H_2	2.68	Aspen Plus Model	H_2 heating pre-DRI (VRE_{off}) + [H_2 for DRI x (VRE_{off} (hrs)/24)]
		SC3				H_2 heating pre-DRI (VRE_{off}) + EAF (VRE_{off}) + casting (VRE_{off}) + [H_2 for DRI x (VRE_{off} (hrs)/24)]
	NH_3	SC1				H_2 for NH_3 synthesis power (VRE_{off}) + H_2 as synthesis feed (VRE_{off})
		SC2				H_2 for NH_3 synthesis power (VRE_{off}) + H_2 to be synthesised (VRE_{off}) + H_2 heating pre-DRI (VRE_{off}) + [H_2 for DRI x (VRE_{off} (hrs)/24)]
		SC3				H_2 for NH_3 synthesis power (VRE_{off}) + H_2 to be synthesised (VRE_{off}) + H_2 heating pre-DRI (VRE_{off}) + EAF (VRE_{off}) + casting (VRE_{off}) + [H_2 for DRI x (VRE_{off} (hrs)/24)]

H_2 compression pre-DRI	LH_2, NH_3	SC2,3	t steel	0.06	Aspen Plus Model	steel produced x (VRE_{on} (hrs)/24))
H_2 heating pre-DRI (VRE_{on})	LH_2, NH_3	SC2,3	t steel	0.45	Aspen Plus Model	steel produced x (VRE_{on} (hrs)/24))
EAF (VRE_{on})	LH_2, NH_3	SC3	t steel	0.75	Kruger et al. (2020)	steel produced x (VRE_{on} (hrs)/24))
Casting (VRE_{on})	LH_2, NH_3	SC3	t steel	0.01	IEA Environmental Projects (2013)	steel produced x (VRE_{on} (hrs)/24))

H_2 for feedstock (AU/JP): *$H_{2,annual}$ (t H_2) = demand rate (kg H_2/t) x quantity (t) x 10^{-3}*

Applicable processes	Energy vector	SC	Unit	Demand (kg H_2)	Source	Qty (annual basis)
DRI	LH_2, NH_3	SC1,2,3	t steel	51.98	Aspen Plus Model	steel produced

H_2 or NH_3 for heat (AU/JP): *$H_{2,annual}$ (t H_2 or NH_3) = demand rate (kg H_2 or NH_3/t) x quantity (t) x 10^{-3}*

Applicable processes	Energy vector	SC	Unit	Demand (kg H_2 or NH_3/unit)	Source	Qty (annual basis)
NH_3 cracking	NH_3	SC1	t steel	5.98 kg NH_3	Aspen Plus Model	steel produced
H_2 heating pre-DRI (JP)	LH_2	SC1	t steel	15.75 kg H_2	LHV-based combustion calculation with 85% efficiency	steel produced
	NH_3	SC1		101.59 kg NH_3		steel produced
H_2 heating pre-DRI (VRE_{off})	LH_2, NH_3	SC2,3		15.75 kg H_2		steel produced x (VRE_{off} (hrs)/24))

H_2 for power (AU): *$H_{2,annual}$ (t H_2) = demand rate (kg H_2/t) x quantity (t) x 10^{-3}*

Applicable processes	Energy vector	SC	Unit	Demand (kg H_2/unit)	Source	Qty (annual basis)
NH_3 synthesis (VRE_{off})	NH_3	SC1	t NH_3	34.94 (2030) 32.76 (2050)	Nayak-Luke et al. (2018) for power required + FC efficiency	H_2 for export and shipping fuel x (VRE_{off} (hrs)/24)
EAF (VRE_{off})	LH_2, NH_3	SC3	t steel	37.58 (2030) 35.23 (2050)	IEA Environmental Projects (2013) for power required + FC efficiency	steel produced x (VRE_{off} (hrs)/24))
Casting (VRE_{off})	LH_2, NH_3	SC3	t steel	0.52 (2030) 0.48 (2050)	IEA Environmental Projects (2013) for power required + FC efficiency	steel produced x (VRE_{off} (hrs)/24))

H_2 or NH_3 for power (JP): *$H_{2,annual}$ (t H_2 or NH_3) = demand rate (kg H_2 or NH_3/t) x quantity (t) x 10^{-3}*

Applicable processes	Energy vector	SC	Unit	Demand rate (kg H_2 or NH_3/unit)	Source	Qty (annual basis)
H_2 compression pre-DRI	LH_2, NH_3	SC1	t steel	3.23 kg H_2 (2030) 3.03 kg H_2 (2050) 20.82 kg NH_3 (2030) 19.52 kg NH_3 (2050)	Aspen Plus Model for power required + FC efficiency	steel produced
EAF	LH_2, NH_3	SC1,2	t steel	37.58 kg H_2 (2030) 35.23 kg H_2 (2050) 242.47 kg NH_3 (2030) 227.32 kg NH_3 (2050)	Kruger et al. (2020) for power required + FC efficiency	steel produced
Casting	LH_2, NH_3	SC1,2	t steel	0.52 kg H_2 (2030) 0.48 kg H_2 (2050) 3.32 kg NH_3 (2030) 3.11 kg NH_3 (2050)	IEA Environmental Projects (2013) for power required + FC efficiency	steel produced

H_2 or NH_3 for mobility (JP): *$H_{2,annual}$ (t H_2 or NH_3) = demand rate (t H_2 or NH_3/t) x quantity (t)*

Applicable processes	Energy vector	SC	Unit	Demand rate (kg H_2 or NH_3/unit)	Source	Qty (annual basis)
Dry bulk carrier, Newcastlemax	LH_2	SC1	Journey (return trip)	250.34 kg H_2 (2030) 236.43 kg H_2 (2050)	Refer to shipping fuel consumption calculations	no. journeys
	NH_3			1479.22 kg NH_3 (2030) 1397.04 kg NH_3 (2050)		
Dry bulk carrier, panamax	LH_2	SC2,3		139.90 kg H_2 (2030) 132.12 kg H_2 (2050)		
	NH_3			826.63 kg NH_3 (2030)		

				780.70 kg NH_3 (2050)		
Liquefied gas tanker	LH_2	SC1,2		289.17 kg H_2 (2030) 273.11 kg H_2 (2050)		
	NH_3			1708.68 kg NH_3 (2030) 1613.75 kg NH_3 (2050)		

Efficiency parameters are summarised in Table A.6, of which the electrolysis and fuel cell efficiencies have already been applied in the preceding Table A.5. The symbol (~) indicates no change between 2030 and 2050.

Table A. 6 – Process efficiency parameters

Parameter	2030	2050	Applicable processes
Electrolyser efficiency (H_2 LHV)	68%	75%	- Water electrolysis for H_2 production
Stationary fuel cell efficiency (H_2 or NH_3 LHV)	60%	64%	- Power demands for inflexible processes, following CGH_2 storage in AU: NH_3 synthesis, EAF and casting - Power demands in Japan: H_2 compression pre-DRI, EAF, casting
Mobile fuel cell efficiency (H_2 or NH_3 LHV)	68%	72%	- Shipping
Inverter efficiency (electrical)	95%	~	- Between direct VRE DC power supply and AC processes in AU: NH_3 synthesis, EAF, casting, H_2 heating pre DRI (AU-VRE_{on}), CGH_2 storage compression and H_2 compression pre-DRI. - Between SOFC power supply (following CGH_2 storage) and AC processes in AU: NH_3 synthesis, EAF and casting - Between SOFC/PEMFC power supply and electric motors on-board shipping vessels - Between SOFC power supply (following LH_2/NH_3 storage) and AC processes in JP: H_2 compression pre-DRI, EAF, casting.
Thermal heating efficiency (H_2 or NH_3 LHV)	85%	~	- H_2 heating pre-DRI (AU-VRE_{off} and JP) - NH_3 cracking
Electrical heating efficiency (electrical)	90%	~	- H_2 heating pre-DRI (AU-VRE_{on})
LH_2 shipping efficiency (in terms of BOG mass losses at 0.2%/day)	98.21%	~	- Shipping fuel for liquefied gas tankers - LH_2 exports, transported in liquefied gas tankers
	97.81%	~	- Shipping fuel for dry bulk carriers
NH_3 shipping efficiency (in terms of BOG mass losses at 0.02%/day)	99.82%	~	- Shipping fuel for liquefied gas tankers - NH_3 exports, transported in liquefied gas tankers
	99.78%	~	- Shipping fuel for dry bulk carriers
H_2 regasification	100%	~	- LH_2 (at -253°C) or LNH_3 (at -33°C) utilisation in Japan (considered burden free, enabled by an air exchanger)

A.6 Net present value calculations

For all economic data, if literature did not define the cost year, the publication year was assumed to convert to AUD 2020. Unless stated otherwise, exchange rates of 0.73 USD/AUD and 0.64 EUR/AUD were applied (2016-2020 average, Reserve Bank of Australia (2021)).

CAPEX and OPEX were subject to a discount factor:

$$f_d = \frac{1}{(1+i)^N} \qquad (A.14)$$

where i = real discount rate (%) and N = number of years.

All discounted cash flows over project lifetime were summed to give NPV ($), then the annualised cost (C_{ann}) calculated:

$$C_{ann,\,total}\ (\$/yr) = CRF \times NPV_{total} \qquad (A.15)$$

$$where\ CRF = \frac{i(1+i)^N}{(1+i)^N - 1}$$

LCOS for one tonne of semi-finished steel was determined by:

$$LCOS\ (\$/t) = C_{ann,\,total} \div S \qquad (A.16)$$

where S = annual steel production (t)

$LCOH_p$ costs could similarly be derived:

$$LCOH_p\ (\$/kg) = C_{ann,\,Hp} \div H_p \qquad (A.16)$$

where $C_{ann,\,Hp}$ = CRF x NPV_{Hp} , H_p = annual hydrogen production (kg) and NPV_{Hp} = discounted cash flows from relevant CAPEX (electrolyser) and OPEX (electricity, water, labour)

A.7 Charter rate calculations

Charter rates were determined based on the vessel, propulsion system and fuel storage CAPEX plus the OPEX of crew, port fees, consumables, maintenance, repair, and insurance.

$$c_{bulk\ carrier}\ (\$/day) = (CAPEX + (OPEX \times l)) \div (l \times d) \qquad (A.17)$$

where:
CAPEX = capital expenditure ($), including vessel, fuel cell, electric motor, and fuel storage costs (various sources, data in Table A.8), plus a total investment cost of 10%
OPEX = operational expenditure ($/year), extracted from (Delhaye et al., 2010)
l = lifetime (years), taken as 25 years (Kretschmann et al., 2017)
d = days spent at sea (days/year)

$$c_{gas\ tanker}\ (\$/day) = (CAPEX + OPEX) \div (lifetime \times d) \qquad (A.18)$$

where:
CAPEX (inc. investment cost), OPEX and lifetime are given by Al-Breiki and Bicer (2020a), d = days spent at sea (days/year)

Bulk carrier costs were differentiated by fuel cell improvements between 2030 and 2050. In the absence of better data, the liquefied gas tanker CAPEX was based on a vessel with ICE propulsion system and bunker fuel storage. To account for the cost reductions as a function of FC improvements, a 5% cost reduction was applied for 2050.

Total cost of charter was then determined by:

$$C_{shipping,\,charter}\ (\$/year) = c \times V \times d \qquad (A.19)$$

where: c = charter rate ($/day), V = number of vessels in fleet, and d = days spent at sea (days/year)

A.8 Infrastructure lifetimes

Based on lifetimes, stationary FCs operating in Australia (during VRE_{off}) required replacement every 16-18 years (2030-2050) whilst those operating in Japan (24-hour operation) were replaced every 10-11 years. Mobile FCs were replaced every 5-6 years which formed part of the shipping charter costs. All FC replacements accounted for 33% of initial investment cost (Taljegard et al., 2014).

Apart from FCs, no other infrastructure had to be replaced within the 20-year project lifetime. Solar panels pertained a service life of 25 years (Poulek et al., 2012), CGH_2, LH_2 and NH_3 plant had a lifetime of 40 years (Bruce et al., 2018) and the DRI-EAF plant had a lifetime of 20 years (Vogl et al., 2018). The alkaline electrolyser lifetime was 95,000 hours in 2030 and 120,000 hours in 2050 (IEA, 2019), and since they operated dynamically during VRE_{on}, this equated to 29 years and 38 years of operation in 2030 and 2050, respectively.

A.9 Labour costs

The labour cost was determined as a function of full time equivalent (FTE) employees, which is summarised in Table A.7.

Table A. 7 – labour-demanding processes and corresponding rates

Process	Rate	Unit	Reference
Electrolysis	0.08	FTE/t H_2 per day	U.S. Department of Energy (DOE) (2012)
DRI	73	FTE/Mt DRI per year	Wood et al. (2020)
EAF	167	FTE/Mt steel per year	
Casting	100	FTE/Mt steel per year	
NH_3 synthesis (exc. electrolysis)	68	FTE/Mt NH_3 per year	
H_2 liquefaction (exc. electrolysis)	386	FTE/Mt H_2 per year	Assumed equivalent to NH_3 synthesis per H_2 output
H_2 compression to 150 bar (exc. electrolysis)	129	FTE/Mt H_2 per year	Assumed 33% of H_2 liquefaction
NH_3 cracking	34	FTE/Mt NH_3 per year	Assumed 50% of NH_3 synthesis

A.10 CAPEX and OPEX data

Table A.8 details CAPEX and OPEX data in 2030 and 2050. Consistently across all plant, maintenance OPEX is taken as 2% of CAPEX. Land purchase costs are not included. The symbol (~) denotes no change in cost within the time interval as the technology is already commercialised.

Table A. 8 – CAPEX and OPEX data

	Cost item	2030	2050	Unit	Reference
CAPEX	VRE system (HomerPro inputs)				
	Solar PV	$ 779	$ 513	A$/kW	Graham et al. (2020)
	Wind	$ 1,812	$ 1,656	A$/kW	Graham et al. (2020)
	Grid (90% renewable)	$ 125	$ 125	A$/MWh	Lu et al. (2017)
	Infrastructure, H2-iron-steel plant				
	DRI shaft furnace	$ 371	~	A$/Mt DRI capacity	Vogl et al. (2018)
	EAF	$ 297	~	A$/Mt steel capacity	Vogl et al. (2018)
	Continuous caster	$ 68	~	A$/Mt steel capacity	IEA Environmental Projects (2013)
	Alkaline electrolyser	$ 884	$ 637	A$/kW	IEA (2019)
	CGH2 compressor + vessel	$ 1,065	~	A$/kg H2/day	Bruce et al. (2018)
	LH2 liquefier + vessel	$ 8	~	A$/kg H2/yr	Bruce et al. (2018)
	NH3 synthesiser + vessel)	$ 1	~	A$/kg NH3/yr	Bruce et al. (2018)
	NH3 cracker	$ 85	~	A$/kg NH3/day	Institute for Sustainable Process Technology (2017)
	SOFC stack - stationary	$ 623	$ 298	A$/kW	Whiston et al. (2019)
	Shipping				
	SOFC stack - mobile	$ 623	$ 298	A$/kW	Whiston et al. (2019)
	PEMFC stack - mobile	$ 117	$ 88	A$/kW	Marcinkoski et al. (2019)
	Electric motor	$ 397	~	A$/kW	de Vries (2019)
	LH2 storage	$ 339	$ 241	A$/GJ	Taljegard et al. (2014)
	NH3 storage	$ 89	~	A$/GJ	Korberg et al. (2021)
	Capesize vessel, excluding propulsion system	$ 34,355	~	A$ thousands/ship	Compass Maritime Services (2021) reduced by 50% for propulsion system and fuel storage
	Panamax vessel, excluding propulsion system	$ 20,209	~	A$ thousands/ship	Compass Maritime Services (2021) reduced by 50% for propulsion system and fuel storage
OPEX	Australian operations				
	Iron ore (2020 average)	$ 149	~	A$/t	World Bank Group (2021)
	Labour	$ 110,476	~	A$/FTE/yr	2019 mean national wage (OECD, 2021) escalated by 30% for steel industry (Wood et al. 2020)
	Water	$ 3	~	A$/kL	International Water Association (2018)
	Japanese operations				
	Labour	$ 78,423	~	A$/FTE/yr	2019 mean national wage (OECD, 2021) using OECD exchange rate of 0.65USD/AUD escalated by 30% for steel industry (Wood et al. 2020)
	Water	$ 1	~	A$/kL	International Water Association (2018)
	LCOE				
	SC1-LH2	$ 57	$ 37	A$/MWh	HomerPro output
	SC2-LH2	$ 58	$ 38	A$/MWh	HomerPro output
	SC3-LH2	$ 59	$ 39	A$/MWh	HomerPro output
	SC1-NH3	$ 60	$ 39	A$/MWh	HomerPro output
	SC2-NH3	$ 60	$ 39	A$/MWh	HomerPro output
	SC3-NH3	$ 59	$ 39	A$/MWh	HomerPro output
	Charter rates				
	Capesize, LH2-PEMFC	$ 26,711	$ 25,880	A$/day	Calculated from shipping CAPEX and OPEX from Delhaye et al., (2010)
	Capesize, NH3-SOFC	$ 29,904	$ 26,775	A$/day	Calculated from shipping CAPEX and OPEX from Delhaye et al., (2010)
	Panamax, LH2-PEMFC	$ 20,144	$ 19,682	A$/day	Calculated from shipping CAPEX and OPEX from Delhaye et al., (2010)
	Panamax, NH3-SOFC	$ 21,895	$ 20,171	A$/day	Calculated from shipping CAPEX and OPEX from Delhaye et al., (2010)
	LH2 tanker	$ 81,349	$ 77,282	A$/day	Calculated from Al-Breiki & Bicer (2020a)
	NH3 tanker	$ 62,664	$ 59,531	A$/day	Calculated from Al-Breiki & Bicer (2020a)

B. Additional Results

B.1 Sankey energy distribution diagrams for 2050

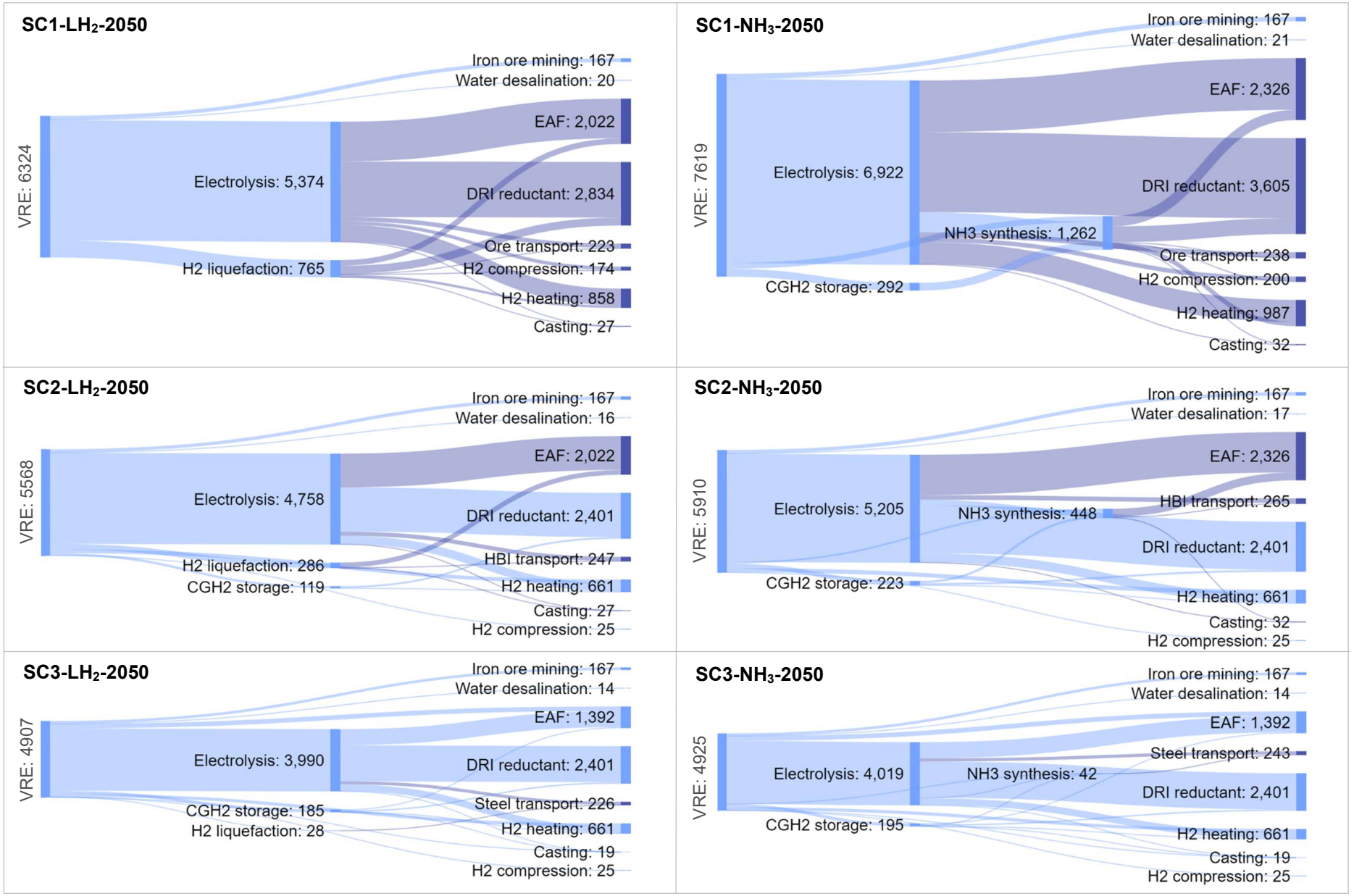

Figure B. 1 – Sankey energy distribution diagrams for 2050 cases (refer to main text, Figure 5 for 2030 cases)

Note: data in kWh/t steel; may not sum due to rounding to nearest whole number; node width correlates to magnitude of energy demand; scale is normalised for all cases.

B.2 Shipping fleets and fuel consumption

Results from equations (A.8) to (A.11), regarding shipping vessel journeys, fleets and departure frequency, are summarised in the table below.

Table B. 1 – Vessel fleet logistics

	Export	Vessel	Journeys (no./year)	Duration, one way (days)	Vessels in fleet (no.)	Departure frequency (days)
SC1	Iron ore	Dry bulk, Capesize	361	11	26	1.0
	LH_2 - 2030	LH_2 tanker	442	9	27	0.8
	LH_2 - 2050		431		27	0.8
	NH_3 - 2030	NH_3 tanker	306	9	19	1.2
	NH_3 - 2050		299		18	1.2
SC2	HBI	Dry bulk, Panamax	717	12	53	0.5
	LH_2 - 2030	LH_2 tanker	159	9	10	2.3
	LH_2 - 2050		149		9	2.4
	NH_3 - 2030	NH_3 tanker	105	9	7	3.5
	NH_3 - 2050		98		6	3.7
SC3	Semi-finished steel	Dry bulk, Panamax	656	12	49	0.6

Results from Equation (A.12) and (A.13) for H_2/NH_3 for mobility described within Table A.5 are summarised in the table below (excludes H_2 liquefaction and NH_3 synthesis).

Table B. 2 – Shipping fuel energy demand

	Shipping fuel energy demand (MWh/t steel)	
	Energy transport (LH_2/NH_3)	**Material transport** (ore/HBI/steel)
SC1 - LH2 - 2030	321	228
SC2 - LH2 - 2030	116	253
SC3 - LH2 - 2030	-	231
SC1 - LH2 - 2050	268	195
SC2 - LH2 - 2050	93	216
SC3 - LH2 - 2050	-	198
SC1 - NH3 - 2030	227	233
SC2 - NH3 - 2030	78	258
SC3 - NH3 - 2030	-	236
SC1 - NH3 - 2050	190	199
SC2 - NH3 - 2050	63	221
SC3 - NH3 - 2050	-	202

B.3 Homer Pro modelling

The 100% VRE system modelled through Homer Pro was completed using the deferrable load module with key inputs, and subsequent results, detailed in Table B.3.

Table B. 3 – Homer Pro data inputs and results

	Inputs				Results		
	Daily load (kWh/d)	Peak load (kW)	Storage capacity (kWh)	storage capacity/ daily load	LCOE (A$/MWh)	CAPEX (A$ millions)	Solar capacity (MW)

SC1 - LH_2 - 2030	807,833,595	89,759,288	807,833,595	100%	57.27	149,951	192,492
SC2 - LH_2 - 2030	681,333,201	75,703,689	553,052,631	81%	58.14	128,543	165,010
SC3 - LH_2 - 2030	572,537,710	63,615,301	411,468,351	72%	58.77	109,179	140,152
SC1 - LH_2 - 2050	669,046,045	74,338,449	669,046,045	100%	37.41	81,560	158,986
SC2 - LH_2 - 2050	586,984,653	65,220,517	468,426,815	80%	38.02	72,732	141,778
SC3 - LH_2 - 2050	515,157,444	57,239,716	363,810,818	71%	38.55	64,693	126,106
SC1 - NH_3 - 2030	918,102,580	102,011,398	608,227,579	66%	60.01	178,800	229,526
SC2 - NH_3 - 2030	706,373,129	78,485,903	463,712,148	66%	59.96	137,566	176,593
SC3 - NH_3 - 2030	572,980,001	63,664,445	401,423,595	70%	59.06	109,844	141,007
SC1 - NH_3 - 2050	810,044,473	90,004,941	534,227,283	66%	39.26	103,888	202,511
SC2 - NH_3 - 2050	624,212,585	69,356,954	407,740,505	65%	39.27	80,055	156,053
SC3 - NH_3 - 2050	517,084,091	57,453,788	356,686,042	69%	38.73	65,280	127,251

B.4 Water and land footprints

Water footprint was assessed, considering both Australia- and Japan-based production. As shown in Table B.4, most of the water demand was for supplying cooling water, where water consumed was a fraction of the water withdrawn. Two return "loops" were considered for water re-use; water consumed for electrolysis at the same rate of release from (i) DRI or (ii) fuel cell power generation (assuming continuous operation with no H_2 losses). The resultant water consumption reduction is only attained if both processes occur in the same location:

- SC2 and SC3: H_2 production (electrolysis) and DRI in Australia
- All excluding LH_2-SC1: H_2 production (electrolysis) and H_2 consumption for power generation in Australia

Table B. 4 – Water-consuming production processes

			L/unit			
Process	**Type**	**Unit**	**Withdrawn**	**Returned**	**Consumed**	**Reference**
VRE production	Cleaning water	MWh	42	0	42	(Jin et al., 2019)
Water electrolysis	Process water	kg H_2	9	0	9	Stoichiometry
DRI	Return water	kg H_2	0	8.55	-8.55	Stoichiometry (+5% losses)
Fuel cell power generation	Return water	kg H_2	0	8.55	-8.55	Stoichiometry (+5% losses)
EAF	Cooling water	t LS	28100	26500	1600	(World Steel Association, 2020c)
Casting	Cooling water	t LS	n/a	n/a	1000	(IEA Environmental Projects, 2013)

Land footprint was quantified for Australia-based production only, due to the dominating spatial factor of solar panels, for which the solar power capacity was determined through Homer Pro modelling. Table B.5 details the land consumption rates for key infrastructure components, including energy storage tanks as energy storage is an potentially important spatial consideration varying with the distinct densities of CGH_2 at 150 bar (11 kg/m3), LH_2 (71 kg/m3) and NH_3 (682 kg/m3) (Bruce et al., 2018; Klüssmann et al., 2020). For calculating the footprints of these storage tanks, a 24-hour capacity was used for each storage, which was deemed sufficient considering the primarily diurnal (as opposed to seasonal) intermittency of VRE and high frequency of shipping vessels leaving Port Hedland (approximately 1 vessel per day; see SI, B.2).

Table B. 5 - Land-consuming processes and corresponding rates

Infrastructure	**m^2/unit**	**unit**	**Reference**
Solar PV panels	28,000	MW	Bruce et al. (2018)
Alkaline electrolysers	95	MW	IEA (2019)
LH_2 spherical storage tank	2.7	t LH_2 (24-hr capacity)	Van Hoecke et al. (2021)
NH_3 storage tank	0.017	t NH_3 (24-hr capacity)	Based on LNG tank, Yang et al. (2006)
CGH_2 storage tank (150 bar)	18.2	t CGH_2 (24-hr capacity)	Bruce et al. (2018)

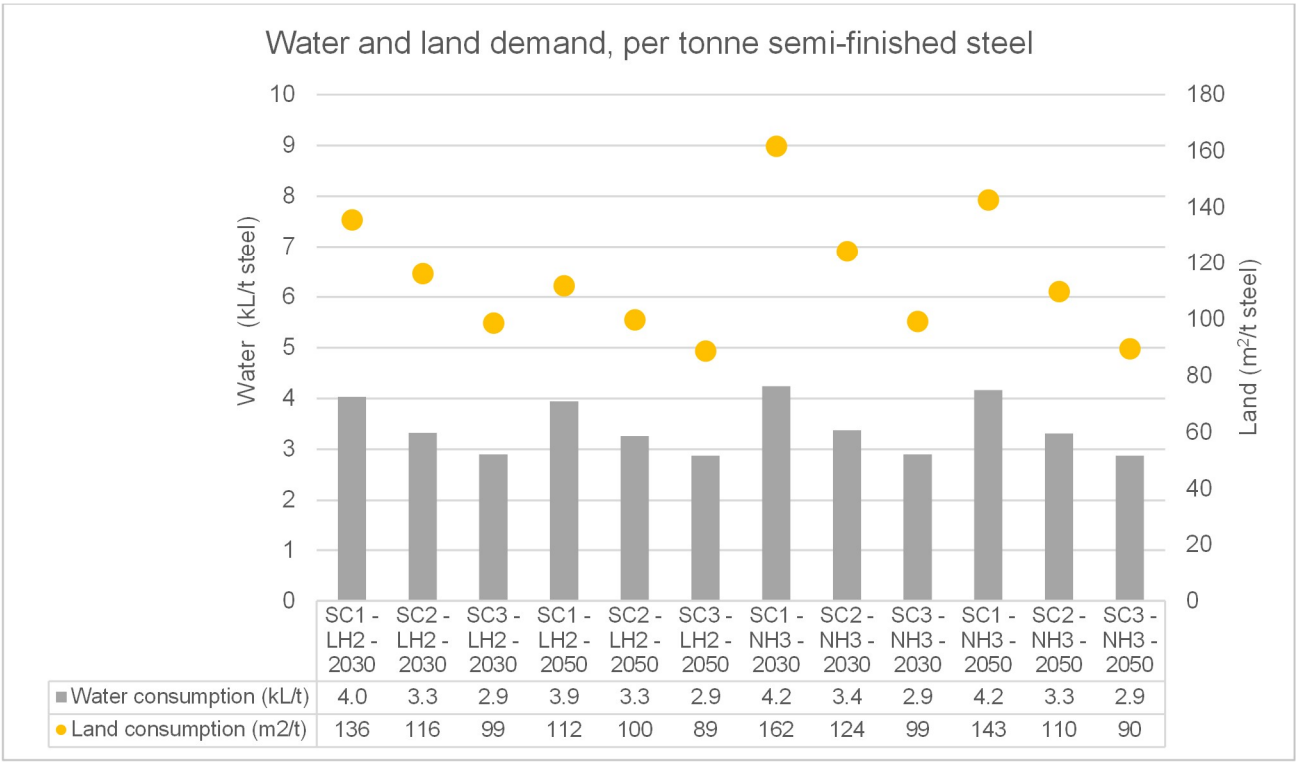

Figure B. 2 - Water and land demand, per tonne of semi-finished steel

B.5 Sensitivity analysis

A sensitivity analysis of key process efficiencies, all varied ±5% from the base case, was carried out on LH_2-2050 and NH_3-2050 cases. The favourable and unfavourable variable inputs are detailed in Table B.6, with results in Figures B.3 and B.4.

Table B. 6 – Sensitivity analysis variables

			Variable			
Process	Case	Basis	Favourable	Base	Unfavourable	Range
Technology in development						
Electrolyser efficiency - 2050	LH_2-2050	% (H_2, LHV)	78.8%	75%	71.3%	+/- 5% to the base case
Liquefaction efficiency - 2050	LH_2-2050	% (H_2, LHV)	86.1%	82%	77.9%	+/- 5% to the base case
FC efficiency - stat - 2050	LH_2-2050	% (H_2, LHV)	67.2%	64%	60.8%	+/- 5% to the base case
FC efficiency - mobile - 2050	LH_2-2050	% (H_2, LHV)	75.6%	72%	68.4%	+/- 5% to the base case
Mature technology (requiring breakthrough)						
EAF	LH_2-2050	MWh/t LS	0.714	0.752	0.789	+/- 5% to the base case
H_2 heating pre-DRI	LH_2-2050	MWh/t LS	0.424	0.446	0.468	+/- 5% to the base case
NH_3 synthesis	NH_3-2050	MWh/t NH_3	0.664	0.699	0.734	+/- 5% to the base case
NH_3 cracking	NH_3-2050	kg H_2 (cracked)/ kg NH_3 (heat)	9.127	8.692	8.257	+/- 5% to the base case

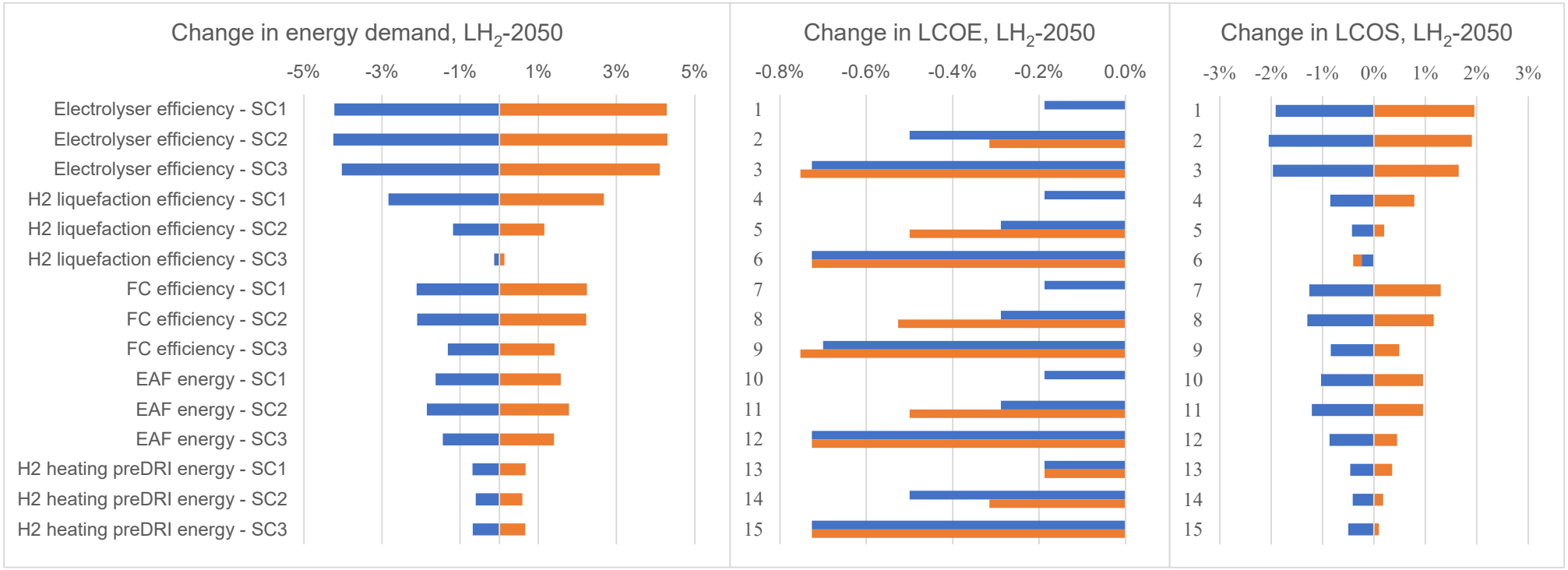

Figure B. 3 – LH_2-2050 sensitivity analysis results for (a) change in energy demand, (b) LCOE and (c) LCOS

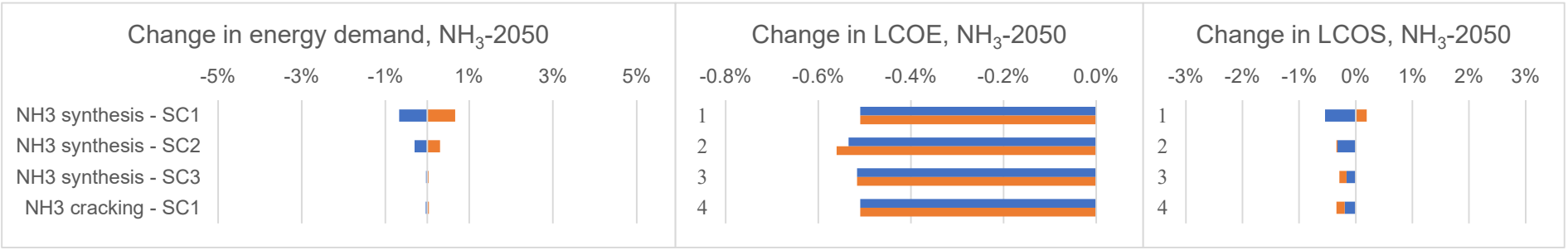

Figure B. 4 – NH_3-2050 sensitivity analysis results for (a) change in energy demand, (b) LCOE and (c) LCOS

References

Al-Breiki, M., & Bicer, Y. (2020a). Comparative cost assessment of sustainable energy carriers produced from natural gas accounting for boil-off gas and social cost of carbon. *Energy Reports*, *6*, 1897-1909. https://doi.org/https://doi.org/10.1016/j.egyr.2020.07.013

Al-Breiki, M., & Bicer, Y. (2020b). Technical assessment of liquefied natural gas, ammonia and methanol for overseas energy transport based on energy and exergy analyses. *International Journal of Hydrogen Energy*, *45*(60), 34927-34937. https://doi.org/https://doi.org/10.1016/j.ijhydene.2020.04.181

Bruce, S., Temminghoff, M., Hayward, J., Schmidt, E., Munnings, C., Palfreyman, D., & Hartley, P. (2018). *National Hydrogen Roadmap*. https://www.csiro.au/en/work-with-us/services/consultancy-strategic-advice-services/csiro-futures/futures-reports/hydrogen-roadmap

Compass Maritime Services. (2021). *Compass Maritime Weekly Report,* . https://compassmar.com/reports/Compass%20Maritime%20Weekly%20Market%20Report.pdf

de Vries, N. (2019). *Safe and Effective Application of Ammonia as a Marine Fuel* Delft University of Technology]. http://resolver.tudelft.nl/uuid:be8cbe0a-28ec-4bd9-8ad0-648de04649b8

Delhaye, E., Breemersch, T., & Vanherle, K. (2010). *The Competitiveness of European Short-Sea Freight Shipping Compared with Road and Rail Transport*. https://www.tmleuven.be/en/project/europeanshortseashipping

Giddey, S., Badwal, S. P. S., Munnings, C., & Dolan, M. (2017). Ammonia as a Renewable Energy Transportation Media. *ACS Sustainable Chemistry & Engineering*, *5*(11), 10231-10239. https://doi.org/10.1021/acssuschemeng.7b02219

Graham, P., Hayward, J., Foster, J., & Havas, L. (2020). *GenCost 2019-20*.

IEA. (2019). *The Future of Hydrogen*. https://www.iea.org/reports/the-future-of-hydrogen

IEA Environmental Projects. (2013). *Iron and steel CCS study: techno-economics integrated steel mill*. International Energy Agency. http://documents.ieaghg.org/index.php/s/P3rYI5vSh80SPM7

Institute for Sustainable Process Technology. (2017). *Power to Ammonia*. https://ispt.eu/media/DR-20-09-Power-to-Ammonia-2017-publication.pdf

International Water Association. (2018). *Total Charge Drinking Water For 188 Cities In 2017 For A Consumption Of 200 M³*. http://waterstatistics.iwa-network.org/graph/8

Kim, K., Roh, G., Kim, W., & Chun, K. (2020). A Preliminary Study on an Alternative Ship Propulsion System Fueled by Ammonia: Environmental and Economic Assessments. *Journal of Marine Science and Engineering*, *8*(3). https://doi.org/10.3390/jmse8030183

Korberg, A. D., Brynolf, S., Grahn, M., & Skov, I. R. (2021). Techno-economic assessment of advanced fuels and propulsion systems in future fossil-free ships. *Renewable and Sustainable Energy Reviews*, *142*, 110861. https://doi.org/https://doi.org/10.1016/j.rser.2021.110861

Kretschmann, L., Burmeister, H.-C., & Jahn, C. (2017). Analyzing the economic benefit of unmanned autonomous ships: An exploratory cost-comparison between an autonomous and a conventional bulk carrier. *Research in Transportation Business & Management*, *25*, 76-86. https://doi.org/https://doi.org/10.1016/j.rtbm.2017.06.002

Krüger, A., Andersson, J., Grönkvist, S., & Cornell, A. (2020). Integration of water electrolysis for fossil-free steel production. *International Journal of Hydrogen Energy*, *45*(55), 29966-29977. https://doi.org/https://doi.org/10.1016/j.ijhydene.2020.08.116

Lu, B., Blakers, A., & Stocks, M. (2017). 90–100% renewable electricity for the South West Interconnected System of Western Australia. *Energy*, *122*, 663-674. https://doi.org/https://doi.org/10.1016/j.energy.2017.01.077

MAN Diesel and Turbo. (2014). *Propulsion Trends in Bulk Carriers*. https://www.mandieselturbo.com/docs/default-source/shopwaredocumentsarchive/propulsion-trends-in-bulk-carriers.pdf?sfvrsn=0

Marcinkoski, J., Vijayagopal, R., Adams, J., James, B., Kopasz, J., & Ahluwalia, R. (2019). *DOE Advanced Truck Technologies*. https://www.hydrogen.energy.gov/pdfs/19006_hydrogen_class8_long_haul_truck_targets.pdf

Nayak-Luke, R., Bañares-Alcántara, R., & Wilkinson, I. (2018). “Green” Ammonia: Impact of Renewable Energy Intermittency on Plant Sizing and Levelized Cost of Ammonia. *Industrial & Engineering Chemistry Research*, *57*(43), 14607-14616. https://doi.org/10.1021/acs.iecr.8b02447

OECD. (2021). *Average annual wages*. https://stats.oecd.org/Index.aspx?QueryName=426&QueryType=View&Lang=en#

Poulek, V., Strebkov, D. S., Persic, I. S., & Libra, M. (2012). Towards 50years lifetime of PV panels laminated with silicone gel technology. *Solar Energy*, *86*(10), 3103-3108. https://doi.org/https://doi.org/10.1016/j.solener.2012.07.013

Reserve Bank of Australia. (2021). *Historical Data*. https://www.rba.gov.au/statistics/historical-data.html#exchange-rates

Taljegard, M., Brynolf, S., Grahn, M., Andersson, K., & Johnson, H. (2014). Cost-Effective Choices of Marine Fuels in a Carbon-Constrained World: Results from a Global Energy Model. *Environmental Science & Technology*, *48*(21), 12986-12993. https://doi.org/10.1021/es5018575

U.S. Department of Energy (DOE). (2012). *DOE Technical Targets for Hydrogen Production from Electrolysis*. https://www.energy.gov/eere/fuelcells/doe-technical-targets-hydrogen-production-electrolysis

Vogl, V., Åhman, M., & Nilsson, L. J. (2018). Assessment of hydrogen direct reduction for fossil-free steelmaking. *Journal of Cleaner Production*, *203*, 736-745. https://doi.org/https://doi.org/10.1016/j.jclepro.2018.08.279

Whiston, M. M., Azevedo, I. M. L., Litster, S., Samaras, C., Whitefoot, K. S., & Whitacre, J. F. (2019). Meeting U.S. Solid Oxide Fuel Cell Targets. *Joule*, *3*(9), 2060-2065. https://doi.org/https://doi.org/10.1016/j.joule.2019.07.018

Wijayanta, A. T., Oda, T., Purnomo, C. W., Kashiwagi, T., & Aziz, M. (2019). Liquid hydrogen, methylcyclohexane, and ammonia as potential hydrogen storage: Comparison review. *International Journal of Hydrogen Energy*, *44*(29), 15026-15044. https://doi.org/https://doi.org/10.1016/j.ijhydene.2019.04.112

Wood, T., Dundas, G., & Ha, J. (2020). *Start with Steel*. Grattan Institute. https://grattan.edu.au/wp-content/uploads/2020/05/2020-06-Start-with-steel.pdf

World Bank Group. (2021). *World Bank Commodities Price Data*. https://thedocs.worldbank.org/en/doc/5d903e848db1d1b83e0ec8f744e55570-0350012021/related/CMO-Pink-Sheet-April-2021.pdf

Yoshino, Y., Harada, E., Inoue, K., Yoshimura, K., Yamashita, S., & Hakamada, K. (2012). Feasibility Study of “CO2 Free Hydrogen Chain” Utilizing Australian Brown Coal Linked with CCS. *Energy Procedia*, *29*, 701-709. https://doi.org/https://doi.org/10.1016/j.egypro.2012.09.082